npg

ORIGINAL ARTICLE

Ultra-diffuse hydrothermal venting supports Fe-oxidizing bacteria and massive umber deposition at 5000 m off Hawaii

Katrina J Edwards[1,2], BT Glazer[3], OJ Rouxel[4,5], W Bach[6], D Emerson[7], RE Davis[8], BM Toner[9], CS Chan[1], BM Tebo[8], H Staudigel[10] and CL Moyer[11]

[1]*Geomicrobiology Group, Marine Environmental Biology Section, Department of Biological Sciences, University of Southern California, Los Angeles, CA, USA;* [2]*Department of Earth Sciences, University of Southern California, Los Angeles, CA, USA;* [3]*Department of Oceanography, University of Hawaii, Honolulu, HI, USA;* [4]*Department of Marine Chemistry & Geochemistry, Woods Hole Oceanographic Institution, Woods Hole, MA, USA;* [5]*Europole Mer, Universite de Bretagne Occidentale, Technopole Brest-Iroise, Place Copernic, Plouzane, France;* [6]*Fachbereich Geowissenschaften, Universität Bremen, Bremen, Germany;* [7]*Bigelow Laboratory for Ocean Sciences, West Boothbay Harbor, ME, USA;* [8]*Division of Environmental and Biomolecular Systems, Oregon Health & Science University, Beaverton, OR, USA;* [9]*Department of Soil, Water, and Climate, University of Minnesota, St Paul, MN, USA;* [10]*Institute of Geophysics and Planetary Physics, Scripps Institution of Oceanography, University of California, La Jolla, CA, USA and* [11]*Department of Biology, Western Washington University, Bellingham, WA, USA*

A novel hydrothermal field has been discovered at the base of Lōihi Seamount, Hawaii, at 5000 mbsl. Geochemical analyses demonstrate that 'FeMO Deep', while only 0.2 °C above ambient seawater temperature, derives from a distal, *ultra-diffuse* hydrothermal source. FeMO Deep is expressed as regional seafloor seepage of gelatinous iron- and silica-rich deposits, pooling between and over basalt pillows, in places over a meter thick. The system is capped by mm to cm thick hydrothermally derived iron-oxyhydroxide- and manganese-oxide-layered crusts. We use molecular analyses (16S rDNA-based) of extant communities combined with fluorescent *in situ* hybridizations to demonstrate that FeMO Deep deposits contain living iron-oxidizing *Zetaproteobacteria* related to the recently isolated strain *Mariprofundus ferroxydans*. Bioenergetic calculations, based on *in-situ* electro-chemical measurements and cell counts, indicate that reactions between iron and oxygen are important in supporting chemosynthesis in the mats, which we infer forms a trophic base of the mat ecosystem. We suggest that the biogenic FeMO Deep hydrothermal deposit represents a modern analog for one class of geological iron deposits known as 'umbers' (for example, Troodos ophilolites, Cyprus) because of striking similarities in size, setting and internal structures.
The ISME Journal advance online publication, 5 May 2011; doi:10.1038/ismej.2011.48
Subject Category: geomicrobiology and microbial contributions to geochemical cycles
Keywords: geomicrobiology; deep biosphere; hydrothermal; iron bacteria; iron oxidation

Introduction

Hydrothermal activity associated with deep-sea volcanism occurs at 'hot-spot' volcanoes such as Lōihi Seamount, Hawaii (Karl *et al.*, 1988) and Vailuluu Seamount, Samoa (Staudigel *et al.*, 2006) and at mid-ocean ridge spreading centers such as Axial Seamount (Johnson and Embely, 1990) and Larson's Seamounts (Alt, 1988). Most hydrothermal

activity occurs close to volcano summits and ridge axes, where significant thermal and chemical anomalies exist (Sakai *et al.*, 1987) due to the intrusion and shallow emplacement of magma. However, there is mounting evidence for off-axis venting: examples include Baby Bare seamount on the eastern flank of the Juan de Fuca Ridge (Wheat and Mottl, 2000), Lost City on the Mid-Atlantic Ridge (Kelley, 2005), with consequence for oceanic elemental budgets (Wheat and Mottl, 2000).

Lōihi Seamount (summit at ∼1000 m below ocean surface) is a seismically active submarine volcano that represents an emerging Hawaiian Island (Klein, 1982; DeCarlo *et al.*, 1983) (Supplementary Figure S1). Venting fluids near the summit of Lōihi (Pele's Pit) are enriched in CO_2, NH_4^+, Si, Fe, alkalinity

and Mn (Sedwick *et al.*, 1992; Wheat *et al.*, 2000). Cm-thick Fe-rich microbial mats at Pele's Pit are highly localized, close to focused hydrothermal venting (Karl *et al.*, 1988; Emerson and Moyer, 2002), and are dominated by neutrophilic Fe-oxidizing bacteria related to the genus *Mariprofundus*, which occurs within a novel class of the Proteobacteria, the *Zetaproteobacteria* (Emerson *et al.*, 2007).

We report 'FeMO Deep', a novel hydrothermal field at 5000 mbsl off the southern flank of Lōihi seamount that is characterized by massive Fe-oxyhydroxide deposition. Chemical, mineralogical, morphological and biological evidence indicate that neutrophilic iron-oxidizing bacteria (FeOB) are responsible for the Fe-oxyhydroxide deposition that results in formation of regionally extensive, mineral-rich microbial mat ecosystems. We refer to the type of hydrothermalism observed at FeMO Deep as *ultra-diffuse*, being characterized by extremely dilute, cooled, distally sourced hydrothermal fluids. Ultra-diffuse hydrothermal fluid venting is expressed as slow leakage on the seafloor, km in size, which is larger than most described hydrothermal vent systems that are characterized by focused flow. The style of Fe-Mn deposition at FeMO Deep (lamination, mineralogy and setting), suggests that the system represents a modern genesis analog for hydrothermal Fe-Mn oxide deposits that are preserved in the geological rock record (for example, umber deposits from the Troodos Ophiolite (Robertson, 1975)).

Materials and methods

Cruises
Sample collection and surveying were conducted on three cruises, with the research vessel (R/V) Melville (Scripps Institution of Oceanography) in 2006 (FeMO 2006), the R/V Kilo Moana (University of Hawaii) in 2007 (FeMO 2007), the R/V Thompson (University of Washington) in 2008 (FeMO 2008) and the remotely operated vehicle (ROV) Jason II (Woods Hole Oceanographic Institution, Woods Hole, MA, USA) in all years. Cruises and operations took place from 24 October to 10 November 2006, 11 October to 27 October 2007 and 22 September to 10 October 2008.

Mat sampling
Mat sampling at FeMO Deep was accomplished using the ROV Jason II suction sampler. This sampler was equipped with five 5 l canisters into which mat was collected. The suction sampler was flushed between sampling different mat. Once retrieved, the canisters were sub-sampled for various chemical, mineralogical and biological analyses.

Electrochemistry
For voltammetry, current is measured while scanning a voltage range, allowing simultaneous detection of multiple chemical species (analogous to varying wavelength and measuring absorbance with spectroscopy). The measured current for peaks detected during voltage scans is proportional to analyte concentration. Many important redox species can be characterized using voltammetry, including O_2, Mn^{2+}, Fe^{2+}, H_2S/HS^-, Sx^{2-}, $S^0_{(aq)}$, $S_2O_3^{2-}$, $S_4O_6^{2-}$, $FeS_{(aq)}$ and aqueous Fe(III)-species. Details regarding construction and analytical methodology for the solid-state working electrodes are available elsewhere (Luther *et al.*, 2008). Briefly, a standard three-electrode cell is used, incorporating an Au/Hg working electrode (0.1 mm diameter), a silver/silver chloride (Ag/AgCl) reference electrode (1 mm diameter) and a platinum (Pt) counter electrode (1 mm diameter). All electrodes are custom-made, and sealed in commercially available polyetheretherketone tubing using epoxy. Linear sweep, cyclic or square wave voltammetry is used, scanning from −0.1 to −1.85 V at a scan rate of 250–10 000 mVs−1. Electrochemical conditioning of the electrode surface between scans removes any chemical species from the surface of the electrode, restoring it for the next measurement. All electrodes are calibrated using a standard Analytical Instrument Systems, Inc. (AIS, Inc., Flemington, NJ, USA) benchtop DLK-60 or DLK-100a electrochemical analyzer following established standardization procedures.

The *in situ* voltammetric measurements were made using an *In situ* Electrochemical Analyzer ISEA™ (AIS, Inc.). A titanium pressure case (30 cm long by 20 cm diameter, rated to >10 000 psi) houses the analyzer consisting of a potentiostat, a four-electrode multiplexer and an internal computer. The pressure case was mounted in the Jason II science basket. Real-time communication with the ISEA from the Jason II shipboard control van was made possible via fiber optic tether and RS-232 cabling. Waterproof bulkhead connectors (Subconn, Inc., North Pembroke, MA, USA) allowed cabled connection between the Jason II 12VDC power source, the RS-232 communication, four voltammetric working electrodes and one counter and reference electrode. We constructed a sensor wand consisting of up to four voltammetric working electrodes and the Jason II temperature probe for survey of hydrothermal fluids and mats. ROV manipulator arm controllers allowed for ∼1 cm vertical resolution profiling across the water-Fe/Mn-oxide crust interface and into the underlying Fe-oxyhydroxide mat. Parameters for individual voltammetric scans were set and scans were visualized in real time. Individual scan analysis takes place using a combination of the manufacturer's software, a custom auto-analysis package, and Matlab (Natick, MA, USA).

Mineralogy
The Ula Nui mat particles that were collected during FeMO 2006 were deposited onto 0.2 μm polycarbonate filters by vacuum filtration and rinsed with purified water to remove seasalt. The polycarbonate filters were mounted for analyses at the micro-X-ray absorption spectroscopy (μ-XAS) beamline 10.3.2 at

the Advanced Light Source, Lawrence Berkeley National Laboratory (Marcus et al., 2004). Large areas (~1 mm²) of the polycarbonate filter were mapped by X-ray fluorescence (XRF) with 10 μm² pixels. Custom beamline software (http://xraysweb.lbl.gov/uxas/Index.htm; Matthew Marcus, Berkeley, CA, USA) was used to correct for fluorescence detector dead time and register individual XRF maps, as well as combine specific fluorescence channels from individual maps into one composite map. The XRF map presented in Supplementary Figure S2A displays the distribution of Fe, Mn and Ca, in red, green and blue, respectively, which was used to choose discrete particles/aggregates having distinct chemical composition, and these particles were then examined by collecting either Fe K-edge X-ray absorption near edge structure (XANES) spectra or Mn K-edge XANES spectra. The Fe and Mn XANES spectra were used to query many particles and gain an understanding of the mineralogical heterogeneity of the mat particulates. Extended X-ray absorption fine structure (EXAFS) spectra were collected from representative particles at the Fe and Mn K-edges. The EXAFS spectra were collected in fluorescence and transmission modes simultaneously. Individual scans were deadtime corrected (fluorescence mode), energy calibrated and averaged. The spectra were processed (pre-edge subtraction, spline subtraction and conversion to k-space) using SixPack software (Webb, 2005). In addition, all XAS locations were revised for XRF spectra and transmission 2-dimensional X-ray diffraction (incident energy 17 keV). The Mn-oxide minerals used as references are acid birnessite (McKenzie, 1971; Villalobos et al., 2003, 2006) and todorokite (Ching et al., 1999). The Fe-oxyhydroxide minerals used as references are Juan de Fuca biogenic (Toner et al., 2009) 2-line ferrihydrite, 6-line ferrihydrite and goethite (Hansel et al., 2003).

Geochemistry

Major (Fe and Mn) and trace element (Co, Ni and Cu) concentrations of mats were determined at WHOI by high-resolution ICP-MS (Thermo-Element II, Thermo Fisher Scientific, Waltham, MA, USA) after complete acid digestion using HNO_3-HCl-HF mixture. Instrumental sensitivity and matrix effects are corrected using an internal standard with a concentration of 5 ppb. Reported concentrations were determined through standardization to the geostandards IF-G and BHVO-1. Selected samples were also sent to Activation Laboratories Ltd (Ancaster, Ontario, Canada) for complementary geochemical analysis. Major and trace elements (including Si) were analyzed in Activation Laboratories by ICP-AES and ICP-MS, respectively, after lithium metaborate/tetraborate fusion.

Electron microscopy

All electron microscopy was conducted on mat samples collected during FeMO 2006. Scanning-electron microscopy was conducted with a JEOL-7000F-LV, equipped with an EDS detector (Peabody, MA, USA). These mat samples were collected by suction sampling and were stored at 4 °C until imaged. Samples were rinsed with distilled water before mounting for observation. The scanning-electron microscopy was operated at 5.0 kV and a working distance of 6.1 mm.

For transmission-electron microscopy, samples were fixed by addition of gluteraldehyde (to 2.5% final concentration). Samples were rinsed in distilled water to remove salt, air-dried and carbon-coated. Analysis was conducted on a Zeiss 10CA TEM (Marine Biological Laboratory, Woods Hole, MA, USA) operated at 100 kV accelerating voltage.

Cell counts

Direct counts of microbial cell numbers were using the fluorescent dye Syto13 (Molecular Probes, Life Technologies, Carlsbad, CA, USA) as previously described (Emerson and Moyer, 2002) during FeMO 2006. Systematic morphological analysis of biologically formed Fe-oxyhydroxides by light microscopy was also carried out as previously described (Emerson and Moyer, 2002).

Bioenergetic calculations

Computations of Fe activity were conducted using EQ3 (Wolery and Jarek, 2003) and a 0–400 °C, 500 bar database assembled with SUPCRT92 (Johnson et al., 1992). Calculated activities of free Fe^{2+} are between 10 and 40 μM within the mat. O_2 activity of 100 μM was assumed for the area immediately below the mat's surface, the Gibbs energy of reaction of -270 to -282 kJ mol^{-1} O_2 for the reaction $Fe^{2+} + \frac{1}{4} O_{2(aq)} + 2\frac{1}{2}H_2O = Fe(OH)_{3(s)} + 2H^+$.

Genomic DNA extraction

The top and bottom mats were collected using the suction sampling device on the ROV Jason II during FeMO 2006. Total genomic DNA (gDNA) was extracted in duplicate using the FastDNA Spin Kit for Soil following the manufacturer's protocol (Qbiogene, Irvine, CA, USA). Extracted gDNA replicates from each mat were pooled and concentrated using Montage PCR centrifugal filter devices (Millipore, Bedford, MA, USA). The gDNAs were then quantified using a Nanodrop ND-1000 spectrophotometer (Nanodrop Technologies, Wilmington, DE, USA) and diluted to 10 ng DNA per μl using filter sterilized 10 mM Tris (pH 8.0).

Clone library construction

Five replicate 50 μl PCRs were performed, each using 50 ng of total gDNA and Bacteria domain universal primers 68F (5′-TNANACATGCAAGTCGR RCG-3′) and 1492R (5′-RGYTACCTTGTTACGACT T-3′), where R is purine analog K, Y is pyrimidine

4

analog P and N is an equal mixture of both analogs at a single position (Glen Research, Sterling, VA, USA). PCR conditions were as previously described (Emerson and Moyer, 2002). The PCR products were visually assayed for size by 1% agarose gel electrophoresis against a 1-kb ladder DNA size standard. The remaining sample was purified using a Montáge PCR centrifugal filter device (Millipore), and cloned with a TA cloning kit following the manufacturer's protocol (Invitrogen, Carlsbad, CA, USA). All putative clones were streaked for isolation and the insert was assayed for size using PCR with the primers M13F and M13R and running the products against a 1 kb size standard by 1% agarose electrophoresis. Plasmids from 81 clones from the top mat and 74 clones from the bottom mat were then end-sequenced using M13F and M13R primers.

Clone library analysis
Clone sequences were trimmed to include 500 bases from the 5' and 3' ends of the SSU rRNA gene. The 3' sequences were then reverse complemented and concatenated to the 3' end of the 5' sequences, forming a final DNA fragment 1000 bases in length. The sequences were imported into the ARB software environment (Ludwig *et al.*, 2004) and aligned to the SILVA reference 92 SSU database using the ARB fast aligner. The sequences were then inserted into the reference tree using the ARB parsimony command and the pos_var_Bacteria_92 filter included with the Silva reference database to determine approximate phylogenetic placements. 16S rRNA gene sequences from this study were submitted to Genbank under accession numbers JF261512-JF261526.

Terminal restriction fragment length polymorphism (T-RFLP) preparation
Three PCR replicates were carried out on the gDNA using identical PCR conditions and primers as described above, with forward primers being labeled with 6-FAM (6-carboxyfluorescein) on the 5' end. PCR products were visually assayed for size by 1% agarose gel electrophoresis against a 1-kb ladder DNA size standard. The remaining fluorescently labeled PCR products were desalted using Montáge PCR centrifugal filter device. PCR products (15 µl) were partitioned into eight aliquots and separately digested overnight with 5 U of *Hae*III, *Hha*I, *Alu*I, *Mbo*I, *Msp*I, *Rsa*I, *Hinf*I and *Bst*UI (New England Biolabs, Ipswich, MA, USA) in a total volume of 30 µl at 37 °C, with the exception of the *Bst*UI reaction, which was incubated at 60 °C. The restriction fragments were desalted using Sephadex G-75 (Amersham Biosciences, Uppsala, Sweden) and dehydrated. Fragments were resuspended in 15 µl formamide and 0.33 µl Genescan ROX-500 internal size standard (Applied Biosystems, Foster City, CA, USA), denatured by heating for 5 min at 95 °C, and separated by capillary electrophoresis using an ABI 3100 genetic analyzer with a 50 cm capillary array using POP6 polymer (Applied Biosystems). Each terminal restriction fragment length polymorphism (T-RFLP) digestion was separated and visualized at least twice to ensure reproducibility of the analysis.

T-RFLP analysis
The fluorescently labeled 5' terminal-restriction fragments (T-RFs) were sized against the Genescan ROX-500 internal size standard using Genemapper v3.7 (Applied Biosystems). Only fragments between 50 and 500 nucleotides were included in the analysis. The clone sequences were digested *in silico* to determine the predicted T-RF sizes for each of the eight restriction enzymes. The predicted T-RFs were then identified on each of the T-RFLP electropherograms.

Fluorescence in situ *hybridization*
Microbial mat samples (1 ml) were fixed in phosphate-buffered saline containing 4% (w/v) paraformaldehyde for 12 h. The mats were then gently rinsed in phosphate-buffered saline without centrifuging and stored in phosphate-buffered saline:ethanol (1:1) at −20 °C. A fluorescence *in situ* hybridization probe specifically targeting all *Zetaproteobacteria* currently stored in Genbank with >1200 nucleotides was designed using the ARB software environment (Ludwig *et al.*, 2004). The probe was designated as Zeta-672 (5'-ACTGCTACACACGGAATT-3') and was labeled with Cy5. A second probe was designed to specifically target phylotypes identified in a clone library constructed, which clustered within the *Planctomycete* division. This probe was designated as Plancto-313 (5'-TGTCTCAGTCCCGATGC-3') and was labeled with 6-FAM. The Bacterial group-specific probe Univ-1390 (5'-GACGGGCGGTGTGTACAA-3') (Zheng *et al.*, 1996) was labeled with Cy3.

A measure of 15 µl of settled mat material or pure cultures of *Mariprofundus ferrooxydans* were centrifuged at $10\,000 \times g$ for 30 s and the supernatant was removed and discarded. Furthermore, 100 µl of molten 0.1% low-melt agarose was cooled to 42 °C and added to the mat pellet. The pellet was gently resuspended and was immediately spread onto the surface of a cleaned microscope slide and allowed to dry for 1 h. Thereafter, 100 µl of lysozyme solution containing 10 mg ml^{-1} lysozyme, 50 mM EDTA, pH 8.0 and 100 mM Tris-HCl, pH 8.0 was added to the dried mat and incubated for 1 h at 37 °C in a humidity chamber to permeabilize the cells (Sekar *et al.*, 2003). The slides were then washed briefly with phosphate-buffered saline to remove any remaining lysozyme solution and allowed to dry for 30 min. Hybridization and washes were carried out as previously described (Gloeckner *et al.*, 1996) in triplicate using 10, 20 or 45% formamide. Cells were then visualized on a Carl Zeiss LSM 510

laser scanning confocal microscope. Cells from hybridizations made with 45% formamide showed little or no fluorescence with either Zeta-672 or Plancto-313 probes, whereas cells from hybridizations made with 10 and 20% formamide fluoresced and were also co-hybridized with the Univ-1390 Bacterial group-specific probe. Hybridizations made with 20% formamide were therefore only used in analysis.

Results and discussion

ROV Jason II dives at 5000 m, southeast of the base of the seamount along the south rift (Supplementary Figure S1) reveal extensive Fe mat deposits overlying and bridging basaltic pillow lavas. A black crust obscures Fe mats before sampling, resulting in a smooth pillow-basalt appearance (Figures 1a and b). Except the occasional small patches of rust-colored Fe-staining on the surface of the black crusts, these mats in most places appear indistinguishable from basalt pillows. This Fe mat, named 'Ula Nui' (meaning 'big red' in Hawaiian), is characterized by a laminated, mineralized, cohesive crust of alternating Fe- and Mn-rich minerals draping between basalts, and cap the underlying flocculent, gelatinous and Fe-rich mat (Figure 1).

Shimmering water is not observed at Ula Nui or at surrounding FeMO Deep mats, and thermal anomalies within mats are not detected in any mat interrogated with Jason II probes (~ 3 dozen). Temperature loggers deployed for 1 day in mat indicate a slight, but robust and stable temperature average of $1.72\,^{\circ}\mathrm{C}$ ($\pm 0.002\,^{\circ}\mathrm{C}$), a $0.23\,^{\circ}\mathrm{C}$ thermal anomaly above average ambient bottom water temperature ($1.49 \pm 0.002\,^{\circ}\mathrm{C}$) (Supplementary Figure S3). Surveys conducted around Ula Nui between 2006 and 2009 reveal a $15\,000\,\mathrm{m}^2$ area where mats occurred from 10's of cm to 1 m depth. Surveys ~ 1 km east of Ula Nui reveal Fe mats that present as mounded structures protruding from the seafloor much like pillow basalts (~ 1 m) (Supplementary Figure S4). The mounded mats have similarly been monitored with temperature loggers, and again reveal a small but robust temperature anomaly above ambient deep seawater temperatures (Supplementary Figure S5).

In-situ voltammetric measurements of O_2, Fe^{2+}, Mn^{2+}, H_2S/HS^-, $FeS_{(aq)}$ and Fe^{3+} as a function of depth within mats indicate depletion of O_2 and elevated Fe^{2+}. These data indicate concomitant upward flow of Fe^{2+} and O_2 depletion with depth, implying active redox processes (Figure 2). Fe^{2+} concentrations within mats are highly anomalous compared with non-hydrothermal deep-sea environments where Fe^{2+} supply (via respiration of Fe(III) oxides) is a diffusive sedimentary process (D'Hondt *et al.*, 2004). Dissolved Mn and sulfur species are below *in-situ* detection limits (5 and $0.1\,\mu\mathrm{M}$, respectively), whereas dissolved Fe species are detected at concentrations up to $150\,\mu\mathrm{M}$. Similar opposing gradients of O_2 and Fe^{2+} are observed repeatedly in mats at FeMO Deep, including the mounded mats (~ 3 dozen measurements such as shown in Supplementary Figures S4 and S5).

A movie depicting profiling and sampling at Ula Nui shows the neutrally buoyant, gelatinous
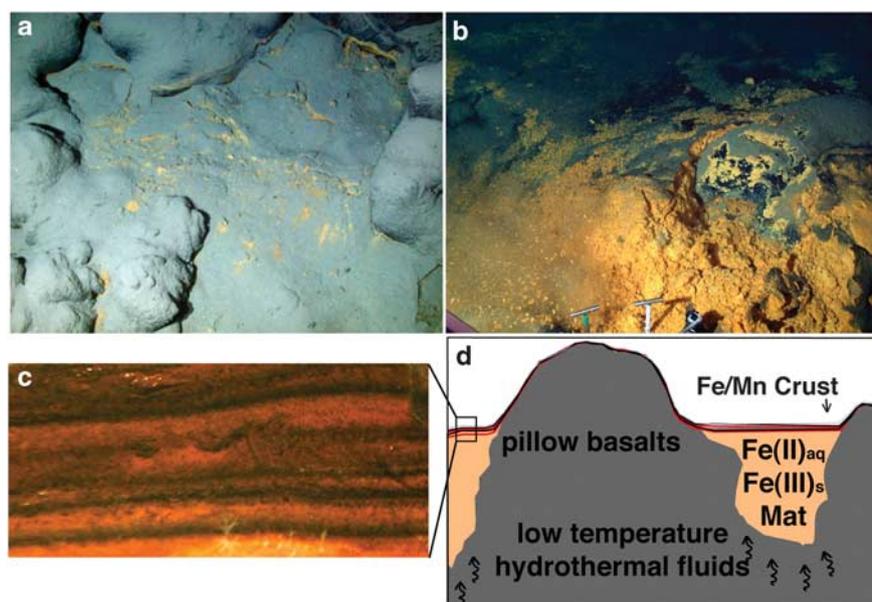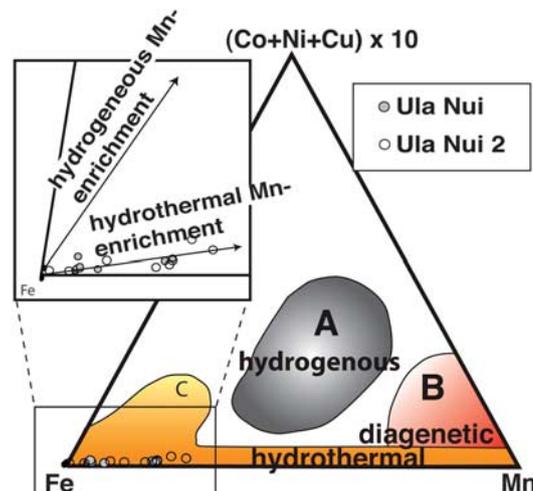

Figure 1 The FeMO Deep mat system. (**a**) Image showing surficial expression of the Fe staining observed at the Ula Nui mat pools before sampling (~ 3 m across). (**b**) Fe Mat revealed after sampling, showing Mn-Fe-rich top crust and underlying Fe mat (~ 3 m across). (**c**) Picture of layered Fe-Mn crust that overlies the Fe-oxyhydroxide-rich mat. (**d**) Model for the Ula Nui mat and other similarly structured (pooled) mats across FeMO Deep based on fluid, mat and crust sampling and electrochemical profiling. Fe-Mn crust is underlain by mat that is from a few centimeters to ~ 1.5 meters in thickness. Although other mat structures (e.g., mounded mats) have been observed at FeMO Deep, the structural style depicted here is the dominant one of which we have made repeated observations and measurements.
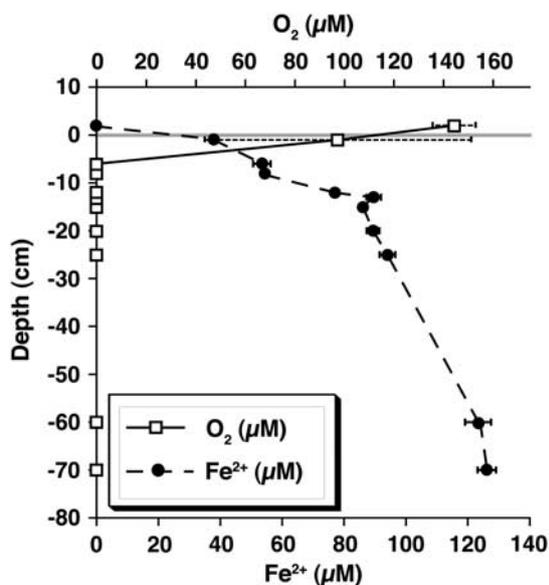
Figure 2 Representative electrochemical profile for the Ula Nui mats. Oxygen is depleted at the mat surface and rapidly drops below detection limit (5 μM) within the first five cm. Oxygen profiles are inversely related to the Fe(II) profiles measured: Fe(II) was not detectable above the mat surface, but starting at the mat surface steadily increases with depth. Error bars associated with detectable oxygen just below the Mn-Fe crust is likely caused by an artifact of the diameter of the sensor wand (~4 cm) and subsequent entrainment of bottom seawater with mat fluids.

Figure 3 Ternary diagram for Mn-Fe-(Co + Ni + Cu) × 10 in Ula Nui mats. The diagenetic, hydrothermal and hydrogenous fields are after Hein *et al.* (1994) and references therein. Ula Nui mat materials are inferred to be solely of hydrothermal origin.

consistency of the Fe mat that underlies the cohesive Fe-Mn crust (Supplementary Movie S1). Chemical analysis of mats indicate high Si content associated with amorphous opal (~10 wt%; Supplementary Table S1 and SOM methods) (DeCarlo *et al.*, 1983; Frey and Clauge, 1983), which is consistent with a hydrothermal source for the Fe-rich mats at Lōihi's summit (DeCarlo *et al.*, 1983) (Supplementary Table S1) and other seamounts. Si is generally enriched in diffuse hydrothermal fluids derived from higher-temperature reactions at depth. Ternary diagrams of Mn-Fe-(Co + Ni + Cu) × 10 are also used to distinguish between hydrothermal and other means of forming Fe-Mn-rich deposit formation, such as chemical precipitation from seawater and hydrothermal plume fall out (Hein *et al.*, 1994). At Ula Nui, the lack of evidence for scavenging of trace metals from seawater (hydrogenous deposition) is consistent with a pure hydrothermal origin (Figure 3), supporting our assessment.

Microscopic examination of the mat reveals various filamentous and spherical mineral structures (Figures 4 and 5). Energy dispersive X-ray analysis indicates that spherical structures are Mn-rich, whereas filamentous structures are Fe-rich (Supplementary Figure S2). Extended X-ray absorption fine structure spectroscopy (EXAFS) at the Fe K- and Mn K-edges for the discrete particles, respectively, indicate that the Fe-oxyhydroxides have less short-range structure than the reference mineral 2-line ferrihydrite, and are more consistent

with biogenic Fe-oxyhydroxides formed at the Juan de Fuca Ridge (Toner *et al.*, 2009) (Figure 6); the Mn oxide has a layer-type structure most similar to triclinic birnessite (Manceau *et al.*, 2002) (Figure 6). The mineralogy and morphologies of the Fe-oxyhydroxide particles in the mat are strikingly consistent with those associated with the activities of known neutrophilic FeOB from Pele's Pit (Emerson and Moyer, 2002), such as the stalks of *Mariprofundus ferrooxydans*, previously isolated from Pele's Pit (Emerson *et al.*, 2007).

T-RFLP and SSU sequence analysis using rRNA clone libraries to identify the prominent groups of bacteria within the mats reveal some similarities between 'Ula Nui and Pele's Pit bacterial populations (Moyer *et al.*, 1995; Figure 7). In particular, phylotypes related to the lithotrophic bacterium *M. ferrooxydans* (Emerson *et al.*, 2007) are detected. Fluorescent *in-situ* hybridizations with group-specific probes demonstrate the presence of live *Zetaprotebacteria* within the Ula Nui mats (Supplementary Figure S6). The prominence of cells that hybridize with probes specific for *Zetaprotebacteria*, together with the morphological evidence cited above, indicates that *Mariprofundus*-like lithotrophs are important constituents of the Ula Nui mat community.

Microbial cell densities measured in the Ula Nui Fe-Mn crust and underlying flocculent mat material range from 6.7×10^8–1.4×10^9 cells per g dry weight, which falls within the range of cell densities detected across mats from the summit region of Lōihi in 2006 (6.5×10^8–2×10^9 cells per g dry weight). An important energy source supporting this microbial community that includes live *Zetaprotebacteria* is Fe^{2+}, which is advected into the mat from below (Figure 2).
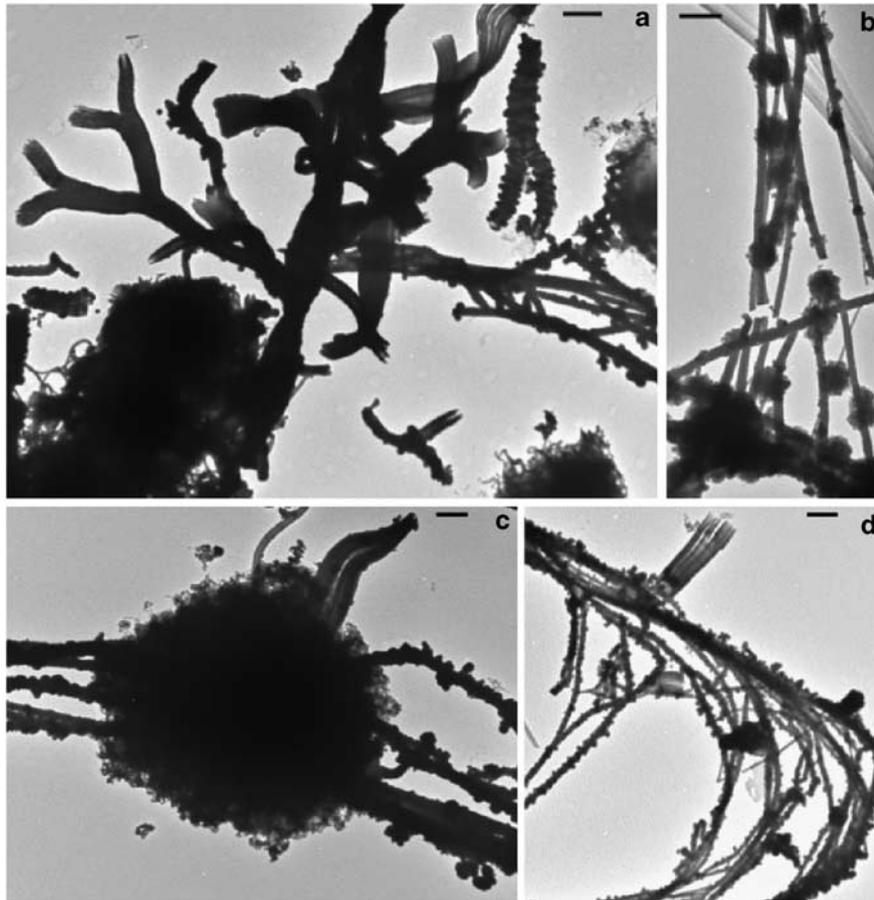
Figure 4 Transmission electron micrographs of the different Fe-oxyhydroxide and Mn oxide particles observed in the Ula Nui mat and crust. (**a**) A variety of branched, twisted, stick-like and spherical materials. (**b**, **c**) Sticks and ball-like structures. (**d**) Bent stick structures. Scale bars: **a**, **c** and **d** = 2 μm; **b** = 1 μm.

We use bioenergetic calculations based on chemolithoautotrophic growth yields for cells sustaining growth based on redox reactions between Fe^{2+} and O_2 to provide estimates of the potential energy that is available for biomass production within FeMO deep mats (Heijnen and Van Dijken, 1992). These calculations indicate that even at very low O_2 activities (1 nM and 1 pM) the reaction is still strongly exergonic (-256 and -240 kJ mol^{-1} O_2, respectively). The electrochemical profiles show that O_2 and not Fe is the limiting reactant, hence, Fe oxidation should be controlled by diffusion of O_2 into the mat. The drop of O_2, from 145 μM outside the mat to <5 μM 5 cm into the mat, indicates a diffusive flux of at least 9×10^6 moles cm^{-2} a^{-1}. This O_2 flux equates to an energy flux of around 2.2 J cm^{-2} a^{-1}. Assuming that aerobic autotrophs require 292 kJ to fix 1 g of biomass (Heijnen and Van Dijken, 1992) and that one cell weighs 10^{-13} g (Whitman *et al.*, 1998), this energy flux could support growth of 8×10^8 cells cm^{-2} a^{-1} and maintain a much greater population. With a mat thickness of 1 m, a fraction of Fe hydroxide filaments (dry weight) of 3% in the mat, and a density of solid $Fe(OH)_3$ of 3.1 g cm^{-3}, we get an average of

10^7 cells g^{-1} dry weight a^{-1}. These numbers are probably higher near the interface with seawater as Fe oxidation there is most rapid. By comparing this conservative number with the actual cell densities, we get turnover times of 20–80 years.

These calculations support the inference that cell densities on the order of 10^7 cells per g dry weight can be expected to grow in a year. Hence, the observed cell densities can be attributed to Fe-oxidation entirely, if the turnover time is 20–80 years, or less so if other energy sources also contribute to cell densities observed, as expected in a natural mat ecosystem. A much larger population based on Fe-oxidation can be supported in maintenance mode ($\sim$3 orders of magnitude (Price and Sowers, 2004) by comparison to that which would be sustained during active growth. Our analyses can only resolve that cells are living, and we cannot infer a specific activity level for these populations—this should be an important further area of research for these novel mats.

The presence of live bacteria related to a known and phylogenetically distinct clade of FeOB and the presence of Fe-oxyhydroxide minerals, which are morphologically and mineralogically consistent
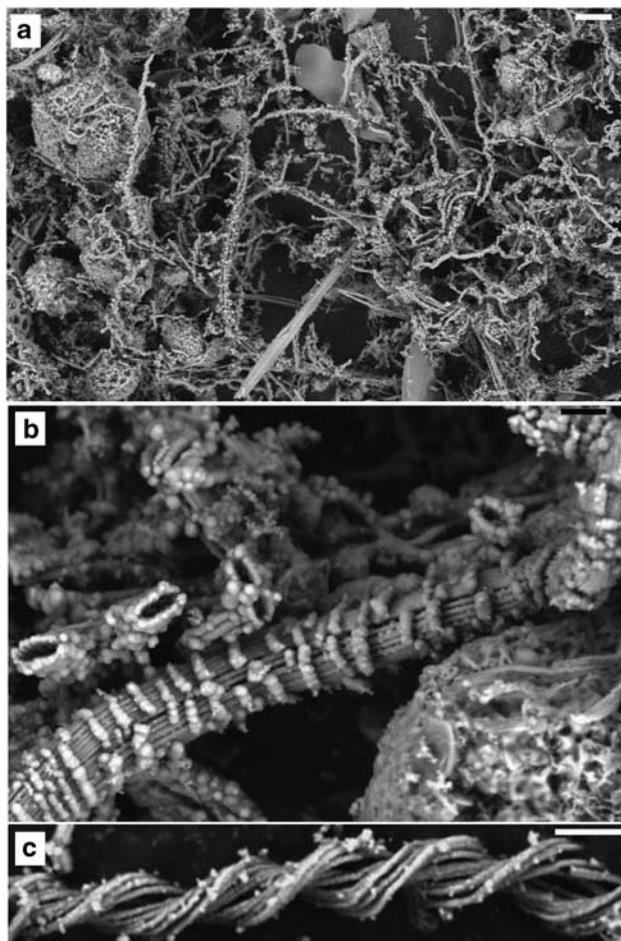
Figure 5 Scanning-electron microscopy micrographs of mat and crust material from Ula Nui. Scale bar for **a** = 10 μm; **b** and **c** = 1 μm. (**a**) Overview of Fe-oxyhydroxide morphologies, including twisted stalk-like structures, spherical structures, long straight stick structures and branching filaments. Mn-oxides occur in spheres of various sizes (μm–mm). (**b**) A higher magnification image, showing some of the more unusual particle morphologies observed; these are thought to be of biogenic origin but have not been commonly reported elsewhere. (**c**) An image of a *Mariprofundus*-style stalk, such as observed at Pele's Pit (Karl *et al.*, 1988; Emerson and Moyer, 2002) and at other marine sites (Juniper and Fouquet, 1988). Among the Fe minerals observed (**a**), a large variation in mineralization (additional mineral accumulation) can been seen; from stalks that appear relatively fresh (**c**) and lacking mineralization to stalks that are very mineralized (**b**), especially by comparison with stalks that are observed from summit sites.

with known bacteriogenic Fe-oxyhydroxides, support our interpretation that these Fe mats are of biological origin. Our chemical measurements further support the hypothesis that this microbial mat is fed by ultra-diffuse advection of hydrothermal fluids, which derive from a higher-temperature source enriched in Fe, Mn and Si that has undergone extensive subsurface cooling. These detectable processes at the seafloor may reflect an abundant deep biosphere harbored in the subsurface, in the cooling and mixing zone beneath the seamount, conditions that would be conducive to supporting microbial life.

Bioenergetic calculations further support our inference that Ula Nui represents a Fe-based, lithotrophic ecosystem. Biological, geochemical and mineralogical data suggest that FeMO Deep mats such as Ula Nui represent a distinct style of ultra-diffuse hydrothermalism, hosting a microbial ecosystem that has an integral role in deposition of laminated, regionally extensive Fe-Mn umber deposits.

Low-temperature Si- and Fe-rich hydrothermal deposits have previously been observed in modern settings (Corliss *et al.*, 1978; DeCarlo *et al.*, 1983; Alt, 1988; Juniper and Fouquet, 1988; Mills *et al.*, 2001). Such vent fields do not generally form Fe-rich deposits at the regional scale of FeMO Deep; rather, they are more similar to the rapidly generated, but highly localized, shallow (a few cm) Fe mats observed at Pele's Pit. However, in contrast to these previous modern-day observations, hydrothermal Si- and Fe-rich deposits that share characteristics with those seen at FeMO Deep are observed in the rock record throughout Earth's history, and some report microfossils of twisted and branching Fe-oxyhydroxide filaments, which are morphologically similar to those found within FeMO Deep mats, and those produced by *Mariprofundus* spp. (Juniper and Fouquet, 1988; Alt *et al.*, 1992; Little *et al.*, 2004; Emerson *et al.*, 2007; Slack *et al.*, 2007). For example, Si- and Fe-rich deposits up to 20 m thick have been reported at ODP Site 801 (Alt *et al.*, 1992) within the Jurassic oceanic crust in the Western Pacific, and numerous fossil hydrothermal Si-Fe-deposits (for example, Jasper and Fe formations) report microfossils in ophiolites as old as 1.74 billion years (Robertson, 1975; Little *et al.*, 2004; Slack *et al.*, 2007). The genetic model for one class of Fe oxide deposits, umbers, has previously invoked deposition of iron and manganese oxides via water-column precipitation of hydrothermal fluids, followed by particle fall out and accumulation in local depressions in a ridge flank setting. However, over the course of the past 30 years of research at deep-sea hydrothermal systems, numerous studies and observations made have failed to reveal modern examples of plume fall out forming umber-like deposits. In contrast, the laminated Fe-Mn structures pooled between pillow basalts observed at FeMO Deep offer an alternative interpretation of umber genesis that is consistent with geological observations.

To our knowledge, FeMO Deep represents the deepest hydrothermal field reported to date, and is the first modern analog of an umber seafloor iron formation in genesis. The discovery of this microbial community at Lōihi and the potential for Fe-based chemosynthetic ecosystems to exist elsewhere in the deep ocean and subseafloor underscores the importance of geomicrobiological interactions in shaping the planetary ecosystem on Earth today, and in the geological past.
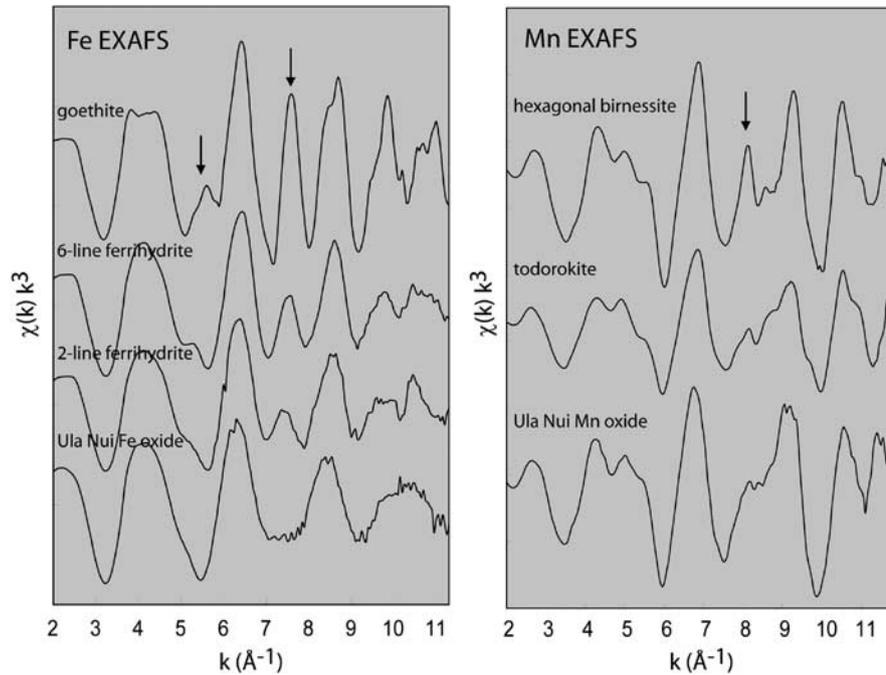
Figure 6 Iron and Mn EXAFS spectra were collected from mineralogically representative Ula Nui mat particles (labeled on XRF map in Supplementary Figure S4A). The Ula Nui Fe oxide spectrum is compared with spectra collected from reference Fe oxide minerals goethite, 6-line ferrihydrite and 2-line ferrihydrite (reference spectra courtesy of Scott Fendorf). The regions of the Fe EXAFS spectra indicated by arrows (at 5.5 and 7.5 Å^{-1}) highlight important spectral features corresponding to mineral structure. The Ula Nui Mn oxide spectrum is compared with spectra from Mn reference minerals hexagonal birnessite (layer-type structure with hexagonal in-layer symmetry) and todorokite (tunnel-type structure, synthesized by Evan Wong). The region of the Mn EXAFS spectra indicated by the arrow highlights a spectral indicator region (7.5–9.5 Å^{-1}) that distinguishes among the various Mn oxide mineral structures. The arrow indicates the spectral feature that identifies the Ula Nui Mn oxide as a triclinic birnessite and distinguishes it from hexagonal birnessite and todorokite.
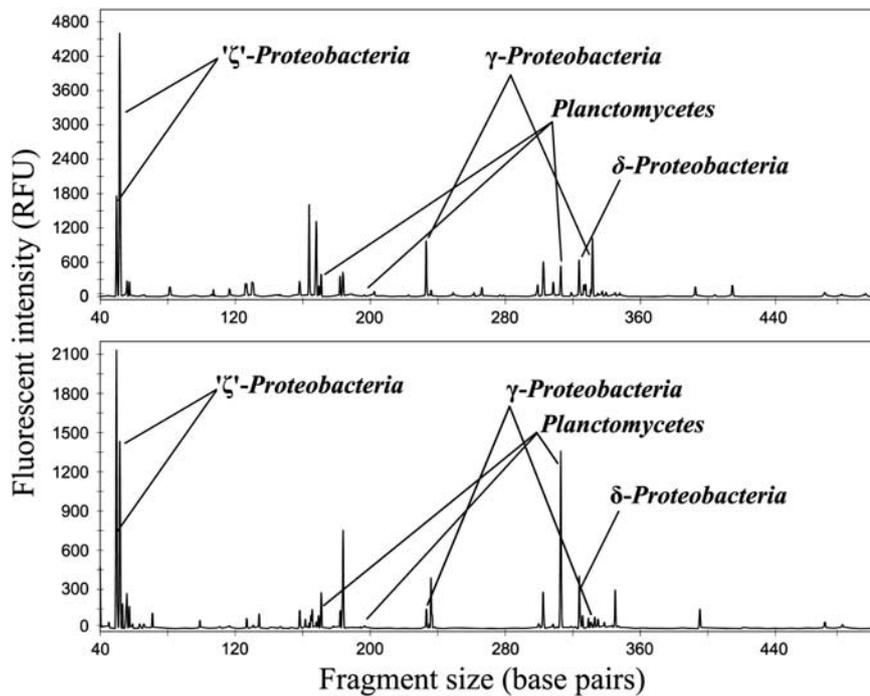
Figure 7 Diversity and relative abundances of the major Bacterial phylotypes detected in Ula Nui microbial mats. Top and bottom panels representing the top and bottom sampled mats, respectively. T-RFLP fingerprints of the SSU rRNA gene indicate that the dominant peaks detected correlate to phylotypes belonging to the *Zetaproteobacteria*, with lesser peaks from the *Planctomycetes*, as well as *Gammaproteobacteria* and *Deltaproteobacteria* (*Hha*I data shown). Peak identification is based on *in silico* analyses using clone library generated sequence information from identical gDNA extractions.

Acknowledgements

References

Alt JC. (1988). Hydrothermal oxide and nontronite deposits on seamounts in the eastern Pacific. *Mar Geol* **81**: 227–239.

Alt JC, Lanord PA, Lloyd PA, Castillo P, Gally A (eds). (1992). *Low-Temperature Hydrothermal Alteration of Jurassic Ocean Crust, Site 801*. Ocean Drilling Program: College Station, TX, pp 415–427.

Ching S, Krukowska KS, Suib SL. (1999). A new synthetic route to todorkite-type manganese oxides. *Inorg Chimica Acta* **294**: 123–132.

Corliss JB, Lyle M, Dymond J, Crane K. (1978). The chemistry of hydrothermal mounds near the Galapagos Rift. *Earth Planet Sci Lett* **40**: 12–24.

D'Hondt S, Jorgensen BB, Miller DJ, Batzke A, Blake R, Cragg BA *et al.* (2004). Distributions of microbial activities in deep subseafloor sediments. *Science* **306**: 2216–2221.

DeCarlo EH, McMurtry GM, Yeh H-W. (1983). Geochemistry of hydrothermal deposits from the Loihi submarine volcano, Hawaii. *Earth Planet Sci Lett* **66**: 438–449.

Emerson D, Moyer CL. (2002). Neutrophilic Fe-oxidizing bacteria are abundant at the Loihi seamount hydrothermal vents and play a major role in Fe oxide deposition. *Appl Environ Microbiol* **68**: 3085–3093.

Emerson D, Rentz JA, Liburn TG, Davis RE, Aldrich H, Chan C *et al.* (2007). A novel lineage of Proteobacteria involved in formation of marine Fe-oxidizing microbial mat communities. *PLoS ONE* **2**: e677.

Frey FA, Clauge DA. (1983). Geochemistry of diverse basalt types from Loihi Seamount, Hawaii: petrogenetic implications. *Earth Planet Sci Lett* **66**: 337–355.

Gloeckner FO, Amann R, Alfreider A, Pernathler J, Psenner R, Trebesius K *et al.* (1996). An *in situ* hybridization protocol for detection and identification of planktonic bacteria. *Syst Appl Microbiol* **19**: 403–406.

Hansel CM, Benner SG, Neiss J, Dohnalkova A, Kukkadapu RK, Fendorf S. (2003). Secondary mineralization pathways induced by dissimilatory iron reduction of ferrihydrite under advective flow. *Geochim Cosmochim Acta* **67**: 2977–2992.

Heijnen JJ, Van Dijken JP. (1992). In search of a thermodynamic description of biomass yields for the chemotrophic growth of microorganisms. *Biotechnol Bioeng* **39**: 833–858.

Hein JR, Hsueh-Wen Y, Gunn SH, Gibbs AE, Chung-ho W. (1994). Composition and origin of hydrothermal ironstones from central Pacific seamounts. *Geochim Cosmochim Acta* **58**: 179–189.

Johnson HP, Embely RW. (1990). Axial Seamount: an active ridge axis volcano on the central Juan de Fuca Ridge. *J Geophy Res* **95**: 12,689–12,696.

Johnson JW, Oelkers EH, Helgenson HC. (1992). SUPCRT92: a software package for calculating the standard molal thermodynamic properties of minerals, gases, aqueous species, and reactions from 1–5000 bars and 0–1000 °C. *Comput Geosci* **18**: 899–947.

Juniper SK, Fouquet Y. (1988). Filamentous iron-silica deposits from modern and ancient hydrothermal sites. *Can Mineral* **26**: 859–869.

Karl DM, McMurtry GM, Malahoff A, Garcia MO. (1988). Loihi seamount, Hawaii—a mid-plate volcano with distinct hydrothermal system. *Nature* **335**: 532–535.

Kelley DS. (2005). A serpentinite-hosted ecosystem: the lost city hydrothermal field. *Science* **307**: 1428–1434.

Klein FW. (1982). Earthquakes at Loihi submarine volcano and the Hawaiian hot spot. *J Geophy Res* **87**: 7719–7726.

Little TS, Glynn SE, Mills RA. (2004). Four-hundren-and-ninety-million-year record of bacteriogenic iron oxide precipitation at sea-floor hydrothermal vents. *Geomicrobiol J* **21**: 415–429.

Ludwig W, Strunk O, Westram R, Richter L, Meiser H, Kumar Y *et al.* (2004). ARB: a software environment for sequence data. *Nuc Acids Res* **32**: 1363–1371.

Luther GWI, Glazer BT, Ma S, Troubworst RE, Moore TS, Metzger E *et al.* (2008). Use of voltammetric solid-state (micro)electrodes for studying biogeochemical processes: laboratory measurements to real time measurements with an *in situ* electrochemical analyzer (ISEA). *Mar Chem* **108**: 221–235.

Manceau A, Marcus MA, Tamura N. (2002). Quantitative speciation of heavy metals in soils and sediments by synchrotron x-ray technique. In: Fenter PA, Rivers ML, Sturchio NC, Sutton SR (eds). *Applications of Synchrotron Radiation in Low-temperature Geochemistry and Environmental Science*. Mineralogical Society of America, 2002, Vol. 49, pp 341–428.

Marcus MA, MacDowell A, Celestre R, Manceau A, Miller T, Padmore HA *et al.* (2004). Beamline 10.3.2 at ALS: a hard X-ray microprobe for environmental and material sciences. *J Synchrotron Rad* **11**: 239–247.

McKenzie RM. (1971). The synthesis of birnessite, cryptomelane and other oxides and hydroxides of manganese. *Mineral Mag* **38**: 493–502.

Mills RA, Wells DM, Roberts S. (2001). Genesis of ferromanganese crusts from the TAG hydrothermal field. *Chem Geol* **176**: 283–293.

Moyer CL, Dobbs FC, Karl DM. (1995). Phylogenetic diversity of the bacterial community from a microbial mat at an active, hydrothermal vent system, Loihi Seamount, Hawaii. *Appl Environ Microbiol* **61**: 1555–1562.

Price PB, Sowers T. (2004). Temperature dependence of metabolic rates for microbial growth, maintenance, and survival. *Proc Nat Acad Sci USA* **101**: 4631–4636.

Robertson A. (1975). Cyprus umbers: basalt-sediment relationships on a Mesozoic ocean ridge. *J Geol Soc Lond* **131**: 511–531.

Sakai H, Tsubota H, Nakai T, Ishibashi J, Akagi T, Gamo T *et al.* (1987). Hydrothermal activity on the summit of Loihi Seamount, Hawaii. *Geochem J* **21**: 11–21.

Sedwick PN, McMurtry GM, MacDougall JD. (1992). Chemistry of hydrothermal solutions from Pele's

Vents, Loihi Seamount, Hawaii. *Geochim Cosmochim Acta* **56**: 3643–3667.

Sekar R, Pernathler A, Pernathler J, Warnecke F, Posch T, Amann R. (2003). An improved protocol for quantification of freshwater Actinobacteria by fluorescence *in situ* hybridization. *Appl Environ Microbiol* **69**: 2928–2935.

Slack JF, Grenne T, Bekker A, Rouxel O, Lindberg PA. (2007). Suboxic deep seawater in the late Paleoproterozoic: evidence from hematitic chert and iron formation related to seafloor-hydrothermal sulfide deposits, central Arizona, USA. *Earth Planet Sci Letters* **255**: 243–256.

Staudigel H, Hart SR, Pile A, Bailey BE, Baker ET, Brooke S *et al.* (2006). Vailulu'u seamount, Samoa: life and death on an active submarine volcano. *Proc Natl Acad Sci USA* **103**: 6448–6453.

Toner BM, Santelli CM, Marcus MA, Wirth R, Chan CS, McCollom TM *et al.* (2009). Biogenic iron oxide formation at mid-ocean ridge hydrothermal vents: Juan de Fuca Ridge. *Geochim Cosmochim Acta* **73**: 388–403.

Villalobos M, Lanson B, Marnceau A, Toner B, Sposito G. (2006). Structural model for the biogenic Mn oxide produced by Pseudomonas putida. *Am Mineral* **91**: 489–502.

Villalobos M, Toner B, Bargar J, Sposito G. (2003). Characterization of the manganese oxide produced by Pseudomonas putida strain MnB1. *Geochim Cosmochim Acta* **67**: 2649–2662.

Webb SM. (2005). SIXPACK: a graphical user interface for XAS analysis using IFEFFIT. *Physica Scripta T* **115**: 1011–1014.

Wheat CG, Jannasch HW, Plant JN, Moyer CL, Samsone FJ, McMurtry GM. (2000). Continuous sampling of hydrothermal fluids from Loihi Seamount after the 1996 even. *J Geophy Res* **105**: 19353–19367.

Wheat CG, Mottl MJ. (2000). Composition of pore and spring waters from baby bare: global implications of geochemical fluxes from a ridge flank hydrothermal system. *Geochim Cosmochim Acta* **64**: 629–642.

Whitman WB, Coleman DC, Wiebe WJ. (1998). Prokaryotes: the unseen majority. *Proc Natl Acad Sci USA* **95**: 6578–6583.

Wolery TJ, Jarek RL. (2003) *Software User's Manual EQ3/6 (version 8.0)*. Sandia National Laboratories: Albuquerque, NM, USA, 2003.

Zheng D, Alm E, Stahl D, Raskin L. (1996). Characterization of universal small-subunit rRNA hybridization probes for quantitative molecular microbial ecology studies. *Appl Environ Microbiol* **62**: 4504–4513.

Supplementary Information accompanies the paper on The ISME Journal website (http://www.nature.com/ismej)